molecular pharmaceutics

Article

Fast biofilm penetration and anti-PAO1 activity of nebulized azythromicin in nanoarchaeosomes

María Julia Altube, Melina MB Martinez, Barbara Malheiros, Paulo C Maffia, Leandro R. S. Barbosa, Maria Jose Morilla, and Eder Lilia Romero

Mol. Pharmaceutics, **Just Accepted Manuscript** • DOI: 10.1021/acs.molpharmaceut.9b00721 • Publication Date (Web): 16 Oct 2019

Fast biofilm penetration and anti-PAO1 activity of nebulized azithromycin in nanoarchaeosomes

Maria Julia Altube [1], Melina MB Martínez[2], Barbara Malheiros[3], Paulo C Maffía[2], Leandro RS Barbosa[3], Maria Jose Morilla[1] and Eder Lilia Romero[1]

1. Nanomedicine Research and Development Centre, Science and Technology Department, National University of Quilmes, Bernal, Buenos Aires, Argentina

2. Laboratorio de Microbiología Molecular, Instituto de Microbiología Básica y Aplicada, Universidad Nacional de Quilmes, Bernal, Buenos Aires, Argentina

3. Institute of Physics, University of São Paulo (USP), São Paulo, Brazil

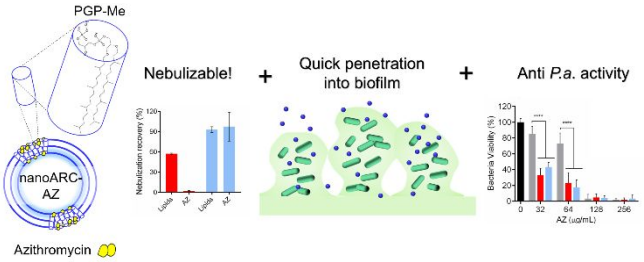
PGP-Me
nanoARC-AZ
Azithromycin
Nebulizable!
+
Quick penetration into biofilm
+
Anti P.a. activity
Nebulization recovery (%)
Bacteria Viability (%)
AZ (ug/mL)

Abstract

Azithromycin (AZ) is a broad-spectrum antibiotic with anti-inflammatory and anti-quorum sensing activity against biofilm forming bacteria such as *Pseudomonas aeruginosa (Pa)*. AZ administered by oral or parenteral routes however, neither efficiently access nor remain in therapeutic doses inside pulmonary biofilm depths. Instead, inhaled nanocarriers loaded with AZ may revert the problem of low accessibility and permanence of AZ into biofilms, enhancing its antimicrobial activity. The first inhalable nanovesicle formulation of AZ: nanoarchaeosome-AZ (nanoARC-AZ) is here presented. NanoARC prepared with total polar archaeolipids (TPA, rich in 2,3-di-O-phytanyl-sn-glycero-1-phospho-(3'-sn-glycerol-1'-methylphosphate) (PGP-Me) from *Halorubrum tebenquichense* archaebacteria, consisted of ~ 180 nm diameter nanovesicles, loaded with 0.28 w:w AZ:TPA. NanoARC-AZ displayed lower MIC and MBC, higher preformed biofilm disruptive and anti-PAO1 activity in biofilm than AZ. NanoARC penetrated and disrupted the structure of PAO1 biofilm within only 1 h. 2 mL of 15 μg/mL AZ nanoARC-AZ nebulized along 5 min rendered AZ doses compatible with *in vitro* antibacterial activity. The strong association between AZ and nanoARC bilayer, combined electrostatic attraction and trapping into perpendicular methyl groups of archaeolipids, as determined by Laurdan fluorescence anisotropy, generalized polarization and SAXS, was critical to stabilize during storage and endure shear forces of nebulization. NanoARC-AZ was non-cytotoxic on A549 cells and human THP-1 derived macrophages, deserving further preclinical exploration as enhancers of AZ anti-PAO1 activity.

Keywords: inhalation, archaeolipid bilayer, antibiotic trapping

1. Introduction

Azithromycin (AZ) is an azalide subclass of macrolide (a semi-synthetic 9- N-methylation derivative of erythromycin), with broad-spectrum antibiotic activity against gram-positive, gram-negative, and atypical bacterial infections that lead to pneumonia.[1,2] AZ is approved by the U.S. Food and Drug Administration (FDA) against pneumonia and chronic obstructive pulmonary disease exacerbations.[2] The *in vivo* effects of AZ combine antibacterial, bronchodilatation and importantly, anti-inflammatory activities (by supressing the activation of NF-kB and the synthesis of proinflammatory cytokines IL-6 and IL-8).[3] The use of AZ extends also to treat chronic lung diseases, where reducing the impact of infection, inflammation and subsequent tissue injury is of major importance.[4] AZ in particular, is administered against inflammatory recurrent chronic airways infections caused by *Pseudomonas aeruginosa (Pa)* [5,6] occurring in cystic fibrosis (CF)[7,8], diffuse panbronchiolitis[9] and bronchiectasis.[10] Long-term treatment with AZ for instance, is included in the current guidelines for CF patients aged ≥ 6 years.[11]

Either to treat pneumonia or chronic lung inflammations, AZ is administered by oral or parenteral routes.[12,4] These systemic routes, however, lead to off-target diffusion, poor bioavailability and, consequently, higher doses to attain the necessary concentrations in the lung, especially in the epithelial lining fluid.[13]

The inhalatory route constitutes a direct pathway to airways, that circumvents the problem of the poor penetration of intravenously administered antibiotics into lung parenchymal tissue and bronchial secretions. It also provides a fast action onset, minimizing the access to circulation and therefore to the generation of unwanted systemic effect.[14] Indeed, different to the intravenous, the inhalatory route is compatible with chronic administration of medicines.[15] AZ moreover, has got poor gastric tolerability in the long term use.[16,17] In view of such circumstances, inhalable formulations of AZ are expected to improve current therapies against lung infections.

The principal weakness of inhaled antibiotics against by *Pa* infections, however, is the low antibiotic exposure in the vicinity of biofilm colonies, a fact that results in diminished anti-pseudomonal efficacy after repeated uses. A suitable nanocarrier for AZ may help to overcome such drawbacks, because of their ability to modify drug's pharmacokinetics, biodistribution and pharmacodynamics (if needed), to selective and efficiently delivery drugs to diseased targets. To that aim however, nanocarriers structure must be tuned as a function of target site and administration route.[18]

Not surprisingly, nanocarriers have started to attract interest as tools to improve the therapeutic index of inhalable antibiotics. Examples of that are the nebulized liposomal ciprofloxacins Pulmaquin and Lipoquin[19], developed by Aradigm[20], and Arikayce, a liposomal amikacin developed by Insmed.[21,22] Arikayce is the first and only medication approved by the FDA for the treatment of *Mycobacterium avium* complex (MAC) lung disease, as part of a combination antibacterial drug regimen for adult patients who have limited or no alternative treatment options.[23] Remarkably, liposomes are the only nanocarriers customized for nebulization, that made it to advanced clinical trials and received FDA approval. The mucus penetrating character of these liposomes enables a prolonged permanence of the antibiotic in the airways, reducing the number of daily administrations. [24]

Despite of the promising avenue opened by inhalable liposomes however, no inhalable liposomal AZ formulations have yet been developed. Approaches based on non-lipid nanocarriers, such as N-fumaroylated diketopiperazine (FDKP) microparticles were recently reported to be used for pulmonary delivery of AZ (AZ@FDKP-MPs), for example. FDKP is an FDA approved, inert excipient used as the primary component in Afrezza® to assist in the delivery of recombinant human insulin via inhalation.[25,26] Compared to intravenous injection and oral administration, intratracheal insufflation of AZ@FDKP-MPs achieved at least a 3.4 times higher local concentration and prolonged retention times.[13] On the other hand, the performance of a liposomal AZ formulation against *Pa* was recently reported to display higher activity than AZ against biofilm forming *Pa in vitro*; the structural features of these liposomes or their administration route however, were not specified.[27] Importantly, the structure of nebulized liposomes must be tailored to avoid structural lability upon nebulization and storage, by adding- as exemplified by Lipoquin and Arikayce bilayers composition -, high proportions of high phase transition temperature lipids, such as HSPC or DPPC, respectively. [28,29]

Nanoarchaeosomes (nanoARC) are soft nanovesicles made of innovative biomaterials, polar lipids extracted from sources other than animal, vegetable, or bacteria: the hyperhalophilic archaebacteria *Halorubrum tebenquichense*. NanoARC are highly resistant to physical-chemistry and enzymatic attacks[30,31] and are also naturally targeted to cells expressing SRA1 (Scavenger receptor

Class AI) nanovesicles, because of their high content on the double negatively charged phosphoarchaeolipid 2,3-di-O-phytanyl-sn-glycero-1-phospho-(3'-sn-glycerol-1'-methylphosphate (PGP-Me), a ligand for SRA1.[32] Recently, we showed that archaeolipids moieties of nebulized pH-sensitive nanoARC used to deliver anti-inflammatory agents to alveolar macrophages, provided higher structural endurance to nebulization stress and storage, than liposomes made of ordinary phospholipids.[32] Because of such benefits, the performance of nanovesicles entirely or partly made of archaeolipids as alternatives to liposomes, is thus worth to be explored. In this work, we hypothesize that AZ loaded nebulized nanoARC made of archaeolipids from *H. tebenquichense* (nanoARC-AZ), may display competitive structural advantages compared to AZ and liposomal AZ. The results showed that nanoARC-AZ, a lacking Chol cholesterol and hydrogenated lipids formulation, proved to be structurally stable upon storage, nebulization, and quickly penetrated PAO1 biofilm displaying higher anti-*Pa* activity than AZ.

2. Materials and methods

2.1 Materials

1,2-Hydrogenated-L-α-phosphatidylcholine (HSPC) was from Northern Lipids Inc, Vancouver, Canadá. Azithromycin dihydrate, cholesterol, 6-Dodecanoyl-N,N-dimethyl-2-naphthylamine (Laurdan), 3-(4,5-dimetiltiazol- 2-yl)-2,5-diphenyl tetrazolium bromide (MTT), phorbol 12-13-acetate (PMA) and 2-mercaptoethanol and mucin from porcine stomach type III were from Sigma-Aldrich (MO, USA). Lissamine™rhodamine B 1,2-dihexadecanoyl-sn-glycero-3-phosphoethanolamine triethylammonium salt (RhPE), Hoechst 33342, Roswell Park Memorial Institute 1640 (RPMI), Dulbecco's Modifed Eagle Medium (DMEM), penicillin-streptomycin sulphate, glutamine, sodium pyruvate and trypsin/ethylenediamine tetra acetic acid were from Gibco® Life Technologies (NY, USA), fetal bovine serum (FBS) was from Internegocios (Buenos Aires, Argentina). Tryptic soy broth (TSB), bacteriological agar and Mueller Hinton Broth (MHB) were acquired from Britania, Buenos Aires, Argentina. The other reagents were of analytic grade from Anedra, Research AG (Buenos Aires, Argentina).

2.2 Archaebacteria growth, extraction and characterization of total polar archaeolipids (TPA)

Halorubrum tebenquichense archaea, isolated from soil samples of Salina Chica, Península de Valdés and Chubut, Argentina was grown in basal medium supplemented with yeast extract and glucose. [33] Biomass was grown in 16.5-L medium in a 25-L homemade stainless-steel bioreactor at 40°C and harvested 72 h after growth. TPA were extracted from biomass using the Bligh and Dyer method modified for extreme halophiles.[34] Between 500 and 700 mg TPA were isolated from each culture batch. The reproducibility of each TPA-extract composition was routinely screened by phosphate content[35] and ESI–MS, as described in Higa et al 2012.[36]

2.3 Preparation of AZ-nanovesicles

Conventional nanoliposomes (HSPC:Chol 3:1 w:w, nanoL), nanoL loaded with AZ (HSPC:Chol:AZ at 0.75:0.25:0.4 and 0.75:0.25:1 w:w, nanoL-AZ), nanoarchaeosomes (TPA, nanoARC) and, nanoARC loaded with AZ (TPA:AZ at 1:0.4 and 1:1 w:w, nanoARC-AZ) were prepared by the film hydration method. Briefly, mixtures of lipids dissolved in chloroform: methanol 1:1 v/v and AZ dissolved in methanol were mixed in round bottom flasks and were rotary evaporated at 40°C until elimination of the solvent. The film was flushed with N_2 and hydrated with aqueous phase (10 mM Tris buffer pH 7.4 with 0.9% w: w, NaCl-Tris buffer) up to a final concentration of 10 mg/mL of total lipids (TL). The resultant suspensions were sonicated (1 h with a bath-type sonicator 80 W, 80 kHz) and extruded 10-times through two stacked polycarbonate membranes of 0.4 and 0.2 µm pore size using a 100 mL Thermobarrel extruder (Northern Lipids, Burnaby, Canada). The resulting nanovesicles were sterilized by passage through a 0.22-µm sterile filter, and stored at 4°C.

To prepare RhPE labelled nanovesicles, RhPE was added at 0.5% weight to the organic lipid solutions, and lipid films were hydrated with NaCl-Tris buffer as stated above.

2.4 Structural characterization of AZ-nanovesicles

Phospholipids were quantified by a colorimetric phosphate microassay.[35]

AZ was quantified by acid derivatization according to Haleem et al.[37] First, samples were disrupted with 200 µL methanol, then 1000 µL hydrochloric acid 11 N was added, and samples were refluxed at 60°C in a water bath for 30 minutes and absorbance was measured at 482 nm. The standard curve was linear in the range of 15 – 100 µg/mL of AZ, with correlation coefficient of 0.9866 ± 0.0042.

RhPE was quantified by spectrofluorometry (λex = 561 nm and λem = 580 nm) using the fluorescence spectrometer LS Perkin Elmer upon complete disruption of 1 volume of nanovesicles in 40

volumes of methanol. The fluorescence intensity (I) of the sample was compared using a standard curve prepared with RhPE in methanol. The standard curve was linear in the range of 0.075–0.5 μg/mL RhPE with a correlation coefficient of 0.9939 ± 0.0025.

Size and ζ potential were determined by dynamic light scattering and phase analysis light scattering, respectively, using a nanoZsizer apparatus (Malvern Instruments, Malvern, UK).

Cryo-electron microscopy (Cryo-EM) was performed at National Laboratory of Nanotechnology (LNNano) at CNPEM - Campinas, São Paulo. A 300 mesh Holey Lacey Carbon grid from Ted Pella® was used, the grids were submitted to a glow discharge procedure (Pelco easiGlow discharge system - Ted Pella, USA) (15 mA for 10 seconds) in order to increase its hydrophilicity. Then grids were inserted in a Vitrobot® (Mark IV, Thermo Fischer Scientific, USA) where 3 μL of sample were added, it was given 20 s for sample fixation. Subsequently, an automatic blotting (blot force=-5, blot total=3) was performed to dry the excess of sample. Finally, the grid was rapidly plunged into liquid ethane wrapped into a liquid nitrogen environment. Measurements were made in a TALOS F200C (Thermo Fischer Scientific, USA) microscope at 200 kV with a CMOS camera Ceta 16M 4K x 4K (Thermo Fischer Scientific, USA). ImageJ® software (National Institutes of Health, 1987) was used to image manipulation.

The order and fluidity of the nanovesicles bilayer with or without AZ were assessed by determining the Laurdan generalized polarization (GP) and fluorescence anisotropy (FA) in the nanovesicles. Nanovesicles were labelled with Laurdan by mixing 10 μL of 120 mM Laurdan in methanol with a volume of nanovesicles sufficient to render a 1: 20 mol: mol Laurdan: lipid ratio. GP was calculated using the following equation:

$$GP = \frac{I_{440} - I_{490}}{I_{440} + I_{490}}$$

where I_{440} and I_{490} are the fluorescence intensities at λem =440 nm and λem = 490 nm, respectively, obtained from the spectra between 400 and 520 nm at λex = 364 nm (slit ex: 5.0 nm and slit em: 10.0 nm. Scan speed: 100 nm min/1). FA was calculated using the fluorimeter software according to the following equation:

$$FA = \frac{I_0 - GI_{90}}{I_0 + 2GI_{90}}$$

where I_0 and I_{90} are the fluorescence intensities at λem = 440 nm with λex = 364 nm, and the excitation polarizer is oriented at 0 and 90° respectively. The correction factor G was obtained from the ratio of emission intensity at 0 and 90°, with the excitation polarizer oriented at 90° (after the subtraction of scattered light).

Small angle x ray scattering (SAXS) measurements were performed at the SAXS1 beam line in the Brazilian Synchrotron Light Laboratory, (LNLS- Campinas, São Paulo, Brazil). The X-ray wavelength was λ=1.488 Å, and the sample-to-detector distance was ~1000 mm, allowing a q-range of $0.1 < q < 4$ nm^{-1}. A bidimensional detector was used (Pilatus 300K). Samples were measured in a mica sample holder, with a 1 mm spacer, temperature was set to 22.0 ± 0.5 °C and controlled with a water bath. Data was collected for 100 s and checked for radiation damage (by measuring consecutive frames). Herein no radiation damage effect was observed during the experiments. Finally, curves were subtracted from the buffer's contribution and normalized by samples' attenuation.

In order to get more information on the scattering curves of this vesicles in the absence and presence of AZ, the uni- and multilamellar model for lipidic vesicles were used (S. 1).[38,39]

2.5 Antimicrobial activity of AZ-nanovesicles

2.5.1 Bacterial strains

Staphylococcus aureus ATCC 25923 (*S. aureus)* and *P.a. ~~P. aeruginosa~~* PAO1 were grown in lysogeny broth (LB) medium in shaking incubator at 37°C and 200 rpm for 18 h until bacterial cultures grew into log phase with optical densities (OD_{600}) ranging from 0.6-0.8.

2.5.2 Minimal inhibitory concentration (MIC) and minimal bactericidal concentration (MBC) assay

MICs were determined by using the broth microdilution assay following the Clinical and Laboratory Standards Institute recommendations.[40] Two-fold serial dilutions of AZ or AZ-nanovesicles were made in cation-adjusted MHB (CAMHB) and added in 96 wells plates. The bacteria inoculum was diluted in CAMHB to obtain a suspension containing approximately 5 x 10^5 colony-forming unit (CFU)/mL and the

plates were incubated for 24 h at 37°C. The MIC was defined as the lowest concentration that completely prevented cell growth detected by the unaided eye.

MBCs were determined by inoculating the wells with samples concentrations above the MIC, on LB agar plates and incubating for 24 h at 37°C. MBC was defined as the lowest concentration producing a 99.9% reduction in CFU relative to the initial inoculum.

2.5.3 Inhibition of biofilm formation

Inhibition of biofilm development was assayed in 96-wells flat-bottom polystyrene plates. AZ or AZ-nanovesicles were two-fold serially diluted in CAMHB and then the bacterial inoculum was added to reach a final concentration of $5x10^5$ CFU/ml, with a final volume of 100 µL per well. Plates were incubated at 37°C for 24 h. Media alone or media with inoculum were used as negative and positive control, respectively. To determine the amount of biofilm, after incubation the supernatant was gently removed, and the formed biofilms were washed twice with 100 µL of saline solution to withdraw planktonic cells. The remaining biofilm was fixed with 100 µL of 100 % methanol for 15 min, and then stained with 100 µL of crystal violet 1% (v/v) for 5 min. The dye was removed and washed twice with 200 µL of distilled water, and the plate was dried at 37°C for 30 min. Finally, 100 µL of 33% (v/v) acetic acid was added, samples were homogenized by gentle agitation and absorbance was measured in a microplate reader at 595 nm.

2.5.4 Disruption of pre-formed biofilm and bacterial viability

Biofilms were developed in 96-wells flat-bottom polystyrene plates with CAMHB broth for 24 h. Then, the supernatant was removed and 100 µl of fresh media with two-fold serial dilutions of AZ or AZ-nanovesicles were added to each well. Plates were incubated for other 24 h at 37°C. Two identical plates were prepared for each experiment. One was used for biofilm quantification by the same crystal violet staining method described above. The other was used to analyze cell viability within biofilm by the formazan dye-based MTT assay. For this purpose, media was gently removed, and biofilms were washed three times with 200 µL of saline. Then, 100 µL of MTT 0.05 % (w/v) was added to each well and plates were incubated at 37°C in the dark for 3 h. After incubation, the supernatant was withdrawn, and formazan crystals were dissolved with 100 µL of dimethyl sulfoxide and homogenized by orbital agitation for 10 min. The absorbance was measured at 570 nm.

2.5.5 Lipase and protease inhibition assays

The bacteria lipase and protease activity were determined as describe Solleti et al.[27] Briefly, AZ and AZ-nanovesicles were diluted in CAMHB at a concentration of 0.25 and 0.5 µg/mL of AZ and transferred in 2 mL tubes. PAO1 suspension was added to the tubes at a final concentration of approximately 5 x 10^5 CFU/mL. Tubes were incubated for 24 h at 37°C and 200 rpm. After 24 h, OD_{600} of each tube was measured; supernatants were collected by centrifugation at 16,000 g and filter sterilized.

For lipase assay a 0.3 mL aliquot of supernatant, 0.3 mL of Tween 20 in NaCl-Tris buffer, 50 µL of $CaCl_2$ (1 M) and 0.6 mL H_2O were mixed in a 2 mL tube and incubated at 37°C for 24 h with agitation at 200 rpm. The presence of lipase was measured by turbidity at OD_{400}. For protease assay, 150 µL of the supernatants were added to the hole of Petri dishes with 25 mL of 2% agar containing 3% skimmed milk and incubated for 48 h at 37°C. The presence of protease was determined by measuring the diameter of the zone of clearance around the holes with calipers.

2.6 Interaction between AZ-nanovesicles and mucins

2.6.1 Nanovesicles size and ζ potential in mucins solution

A mucin solution (mucin at 2.5 % w/v in 8.18 g/L NaCl and 0.37 g/L KCl, pH 7[41] was diluted to 1 mg/mL and incubated with nanovesicles to obtain a relation of 1:1 w:w of mucin:nanovesicles (at a final ratio of 500 µg/mL mucins and 500 µg/mL TL) at 37º C and 200 rpm for 1 h; after that size and zeta potential were determined.[42]

2.6.2 Nanovesicles diffusion through mucins solution

A quantitative diffusion study was performed according to [43,44] using the Transwell system as a two-compartment system. Briefly, 24-wells plates (ThinCert™) with 3 µm pore diameter polyester membrane and occupying a surface of 33.6 mm^2 were covered with 30 mg of mucin solution. The donor chamber was filled with 0.8 mL of RhPE-labelled nanovesicles at 0.5 mg/mL TL in phosphate buffer saline pH 7.2 (PBS). The final mucin concentration was 15 mg/mL in donor chamber. The acceptor compartment was filled with 0.850 mL PBS. The whole plate was covered with a plate lid and incubated at 37°C on an orbital shaker at 300 rpm. At predetermined time points of 0, 1, 4, 10 and 20 h, 100 µL

volumes were removed from the acceptor compartment and replaced by same volume of preheated buffer. The fluorescence intensity of RhPE was measured as stated above.

Percentage of diffusion (*D*) of RhPE-labelled nanovesicles across the mucin layer was calculated according the following equation:

$$D(\%) = \frac{I_{+MUC}}{100 I_{-MUC}}$$

where I_{+MUC} = fluorescence intensity in the acceptor compartment after incubation in the presence of mucins and I_{-MUC}= fluorescence intensity in the acceptor compartment after incubation in the absence of mucins.

2.7 Interaction between nanovesicles and bacteria

2.7.1 Adhesion between nanovesicles and planktonic bacteria

Flow cytometry was used to evaluate nanovesicles-bacterium interactions according to Mugabe et al 2006. Aliquots of overnight bacterial cultures were diluted in phosphate-buffered saline (PBS) and incubated with 25 µg/mL of RhPE-nanovesicles, with or without 5 mg/mL of mucins or PBS alone (control) at 37°C, 200 rpm during 1 h. The samples were centrifuged through a sucrose cushion, washed twice, and fixed with 1% paraformaldehyde. Triplicate samples were then analyzed with FACSCalibur (BectonDickinson, San José, CA, USA). Data were analyzed using Flowing Software 2.5.1 (Finland).

2.7.2 Anti- *P. aeruginosa* activity in the presence of mucins

Bactericidal activities were determined by the microbroth dilution technique. The bacterial strain PAO1 was diluted in CAMHB to obtain 5x10^5 CFU/mL and transferred to 96-well plates. PAO1 was exposed to different dilutions of AZ and AZ-nanovesicles with or without 5 mg/mL of mucins. The plates were incubated for 24 h at 37°C. After incubation, each sample was inoculated on agar plates and incubated for 24 h at 37°C to evaluate bacterial growth by determine CFU/mL

2.7.3 Nanovesicles penetration in *P. aeruginosa* biofilm

To visualize nanovesicles distribution on bacterial biofilm, confocal microscopy analysis was performed according to Dong et al.[45] Briefly, PAO1 biofilm was grown on Nunc™ Lab-Tek™ II Chamber Slide™ (Invitrogen) for 24 h in MHB. Afterwards, the bacterial biofilm on the culture slide was rinsed twice with saline solution to remove the planktonic cells and incubated with RhPE-nanovesicles at 0.5 mg/mL for 1 h and 24 h at 37 °C. Saline solution was applied as the non-treatment control. Biofilms were washed three times with saline solution and stained with 2 µg/mL of Hoechst 33342 for 15 min at room temperature for detection of bacteria. After three washes, biofilms were fixed with glutaraldehyde (5% in PBS). After removing the upper chamber of the culture slide, the samples were sealed with glycerol and ready to be examined under confocal microscope (Olympus FV1000, Japan) with an emission filter of 575–675 nm for RhPE detection (laser 559 nm) and 430–455 nm for Hoechst 33342 detection (laser 405 nm). An objective of 20X (XLUMPLFLN-W) with a NA of 1 was used. For each sample, three representative z-stacks containing the full thickness of biofilm with nanovesicles were captured and experiments were repeated twice. The image processing and analysis were carried out by the software Olympus cell Sens image analysis software v6.3 and three dimensional (3D) reconstructions were generated using Fiji Software.[46]

The penetration of nanovesicles within the biofilm was measured as the relative fluorescence intensity (RFI): RFI = FI RhPE / FF Hoechst

2.8 Cytotoxicity of AZ-nanovesicles of human cells

The human epithelial lung cell line A549 (ATCC® CCL-185™) was bought from Asociación Banco Argentino de Células and were maintained in MEM supplemented with 10 and 20% of FBS, 100 U/mL penicillin, 100 µg/mL streptomycin and 2 mM L-glutamine in a humidified atmosphere of 5% CO_2 at 37°C. Dr Barrionuevo Paula (Instituto de Medicina Experimental, Buenos Aires, Argentina) supplied the human monocyte cell line THP-1 (ATCC TIB-202™). The cells were maintained in complete RMPI medium supplemented with 0.05 mM 2-mercaptoethanol and 1 mM sodium pyruvate. THP-1, monocytes, were differentiated into macrophages by treatment with 100 ng/mL PMA for 24 h.

The viability of cells upon 24 h incubation with empty and with AZ nanovesicles was measured by the MTT assay. Briefly, THP-1 and A549 cells were seeded in 96-well plates with a density of 4 × 10^4 cells per well and grown for 24 h. Then, cells were incubated with series of different concentration of empty nanovesicles (20, 60, 180 and 900 µg/mL of TL), AZ and AZ-nanovesicles (5, 15, 45 and 225 µg/mL of AZ). After 24 h of incubation the medium was removed, cells were washed with PBS and 110 µl of 5 mg/mL MTT solution was added to each well. After 3 hours of incubation, the MTT solution was

removed, the insoluble formazan crystals were dissolved in dimethyl sulfoxide, and absorbance was measured at 570 nm in a Cytation™ 5 Cell Imaging Multi-Mode Reader BioTek Instruments (VT, USA). The cell viability was expressed as a percentage of the cells grown in medium.

2.9 Stability of AZ-nanovesicles upon nebulization

The structural stability of nanovesicles upon nebulization in a vibrating mesh nebulizer (Omron NE-U22, OMRON Healthcare, Japan) was determined in terms of size, polydispersity index, LT and AZ recovery. Briefly, 2 mL of AZ-nanovesicles at a concentration of 15 µg/mL of AZ were nebulized for 5 min. The aerosols were collected in a vessel connected to the nebulizer. Nanovesicles size, TL and AZ were quantified as stated above, before and after nebulization.

2.10 Stability of AZ-nanovesicles upon storage

Empty nanovesicles and AZ-nanovesicles were stored at 4°C for 6 months. Nanovesicles size and ζ potential were determined as stated before, every two months storage

2.11 Statistical analysis

Statistical analyses were performed by one-way analysis of variance followed by Dunnet's test using Prisma 4.0 Software (Graph Pad, CA, USA). The p-value of <0.05 was considered statistically significant: *p < 0.05; **p <0.01; ***p < 0.001, ****p < 0.0001; n.s. represents non-significant (p > 0.05).

3. Results

3.1 Structural features of AZ-nanovesicles

Two types of AZ-nanovesicles were prepared, either starting from 4 or 10 mg/mL AZ. NanoARC-AZ prepared with 4 mg/mL AZ, displayed ~ 69 % TL and ~ 47 % AZ recovery; TL and AZ recovery for nanoL-AZ on the other hand, resulted lower: 69 % and 35 % respectively (Table 1). The ζ potential of nanoARC-AZ was shifted towards a less negative value compared to that of nanoARC, probably because of electrostatic neutralization between negatively charged archaeolipids and positively charged AZ amine groups at pH 7.4. No differences were found in ζ potential of nanoL and nanoL-AZ. AZ-nanovesicles prepared from 10 mg/mL AZ on the other hand, due to their lower TL recovery higher mean size, PDI, and structural instability (AZ precipitation upon stored along 48 h at 4°C) than those prepared with 4 mg/mL, were excluded from further assays.

Table 1. Structural features of nanovesicles

Sample	Initial AZ (mg/mL)	Final AZ (mg/mL)	TL (mg/mL)	AZ/TL (%w/w)	Mean diameter (nm ± SD)	PDI	ζ potential (mV ± SD)	AZ pellet
nanoARC	0		7.6 ± 0.1		182 ± 11	0.18 ± 0.02	-38.7 ± 2.0	
nanoARC-AZ	4	1.9 ± 0.1	6.9 ± 1.4	28 ± 5	168 ± 26	0.23 ± 0.10	-31.2 ± 0.8**	No
nanoARC-AZ	10	4.9 ± 2.2	5.4 ± 0.4	93 ± 47	192 ± 21	0.26 ± 0.01	-31.4 ± 5.2**	Yes
nanoL	0		6.2 ± 0.5		143 ± 4	0.10 ± 0.01	-6.0 ± 0.9	
nanoL-AZ	4	1.4 ± 0.1	6.9 ± 0.5	20 ± 1	172 ± 26	0.17 ± 0.08	-7.1 ± 2.7	No
nanoL-AZ	10	3.6 ± 3.0	4.3 ± 2.4	85 ± 34	260 ± 37****	0.59 ± 0.10****	-5.3 ± 2.4	Yes

Data are expressed as mean ± SD from three independent batches. TL: total lipids; PDI: polydispersity index; SD: standard deviation; Yes: pellet formation after storage at 4°C No: no observation of pellet formation after storage at 4°C. Significant differences were determined between empty and AZ-nanovesicles.

Cryo-EM analysis was performed on AZ-nanovesicles. A representative image of nanoL/nanoL-AZ is shown in Figure 1 (a and b), since no differences were found between the two samples. Overlapped spherical unilamellar and multilamellar structures of sizes between ~50 nm and ~130 nm were observed. Using ImageJ® software, the bilayer thicknesses were estimated in 6.0 ± 0.5 nm medium size, in good agreement with SAXS results (see below). nanoARC are seen in Figure 1 (c and d). A considerable number of unilamellar structures were found accompanied by a few multilamellar structures, in good agreement with SAXS curves. In contrast to nanoARC-AZ, nanoARC displayed rounder morphologies, of sizes variable between ~50 nm and 130 nm, and an estimative medium bilayer thickness of ~4.2 ± 0.5 nm, in good agreement with SAXS results. nanoARC-AZ are seen in Figure 1 (e and f) as mainly unilamellar elliptical nanovesicles, with scarce oligolamellar structures, of sizes between 50 nm and 150 nm mean bilayer thickness of ~ 3.9 ± 0.5 nm, reasonably in accordance with SAXS results.

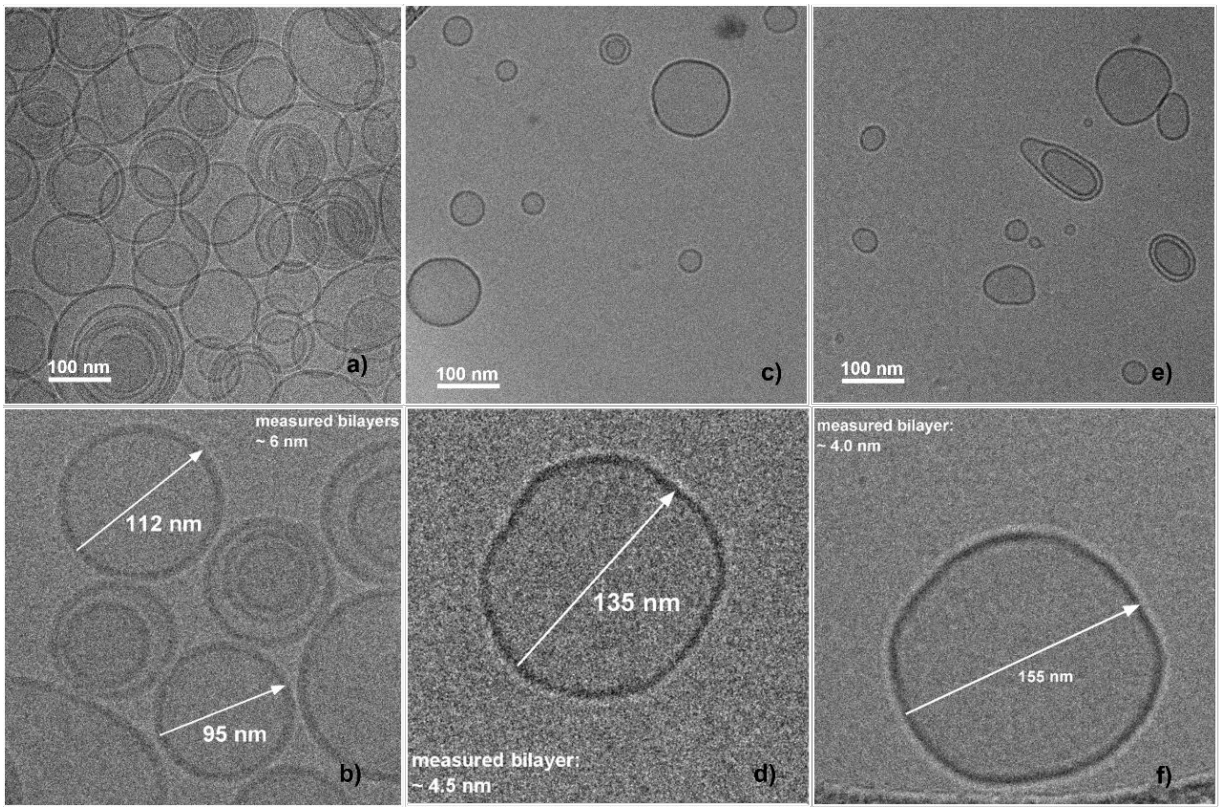

Figure 1. Cryo-EM images of nanoL/nanoL-AZ (a and b), nanoARC (c and d) and nanoARC-AZ (e and f).

The effect of AZ in order or fluidity of AZ-nanovesicles bilayers, was determined by GP and FA of the dye Laurdan, and by SAXS. As shown in Table 2, neither bilayer order nor fluidity were modified in nanoL-AZ, suggesting that AZ was trapped within the aqueous compartment of nanoL. On the other hand, the increased GP of nanoARC-AZ indicated that AZ ordered the nanoARC bilayer; the unchanged FA showed that AZ did not modify its fluidity. The increased order would be owed to AZ partitioning within nanoARC bilayers. These results were confirmed and amplified by SAXS measurements. Figure 2a shows the SAXS curves of nanoL (circles) and nanoL-AZ (squares), without significant changes in the quite well-defined peaks at q ~ 0.085Å^{-1} and ~0.170 Å^{-1} (the scattering curves were vertically shifted to clarify the visualization). The presence of sharp peaks in scattering curves at very specific positions, like the ones reported herein, which is *q* and *2q*, for q ~ 0.085Å^{-1} and ~0.170 Å^{-1}, respectively, is a fingerprint of multilamellar structures. Instead, the SAXS curves of nanoARC (circles) and nanoARC-AZ (squares) in Figure 2b, showed a shift of the first minimum at q ~ 0.045 Å^{-1} to circa q ~ 0.06Å^{-1}, respectively, considered as a clear evidence of structural interaction between AZ and nanoARC bilayers.

Additional structural differences between nanoARC and nanoL were indicated by the absence of multilamellar structures.

Table 2. Laurdan GP and FA of nanovesicles

Sample	GP	FA
nanoARC	-0.455 ± 0.013	0.156 ± 0.011
nanoARC-AZ	-0.337 ± 0.015	0.164 ± 0.002
nanoL	0.385 ± 0.012	0.218 ± 0.001
nanoL-AZ	0.380 ± 0.006	0.215 ± 0.002

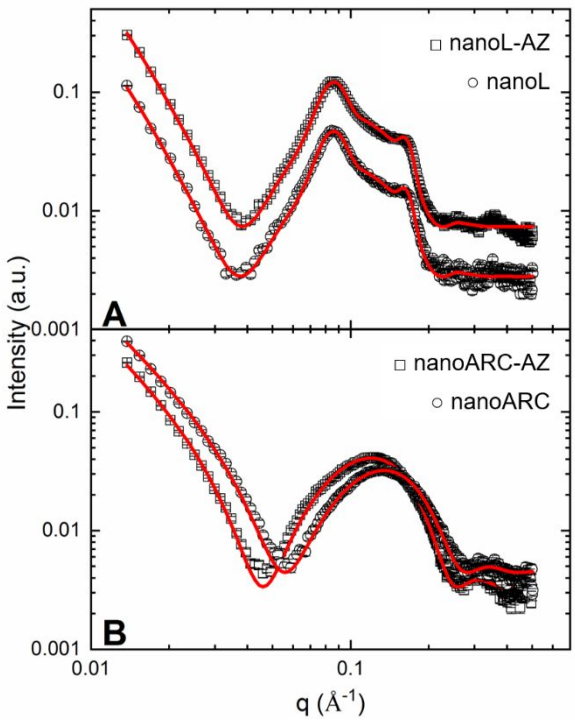

Figure 2: SAXS curves of nanoL [circles], nanoL-AZ [squares] (a) and nanoARC [circles], nanoARC-AZ [squares] (b).

To further characterize the role of AZ into the structure of nanoARC-AZ, the scattering curves of nanoARC and nanoARC-AZ were analysed employing the theoretical model described in section 2.4 (solid lines in Figure 2b). Both scattering curves could be fitted using the well-kwon unilamellar model, already described in the literature.[38,39,47] Our analysis showed that the presence of AZ induced a shrinking in the membrane thickness, that decreased from ~ 48 Å in nanoARC to 43 Å in nanoARC-AZ, respectively. According to the fitting parameters, the most affected structures were the polar heads and the R_{CH_3}region, showing parameters that, in the presence of AZ, decreased from 9.5 Å to 8.2 Å and from 2.9 Å to 1.7Å respectively. Interestingly, AZ did not affect the remaining fitting parameters (Table 3).

Table 3. Small angle scattering fitting parameters from nanoL, nanoL-AZ, nanoARC and nanoARC AZ suspensions in NaCl-Tris buffer.

	nanoL & nanoL-AZ		nanoARC	nanoARC-AZ
	model 1	model 2	--	--
w (%)	0.42 ± 0.01	0.58 ± 0.03	--	--

R_{pol} (Å)	15.6 ± 0.1		9.5 ± 1.0	8.2 ± 0.6
R_{CH_2} (Å)	11.7 ± 0.5		11.4± 1.0	11.4 ± 0.1
R_{CH_3} (Å)	2.5 ± 0.6		2.9 ± 0.8	1.7± 0.4
ρ_{pol} (e/Å^3)	0.41 ± 0.1		0.44 ± 0.02	0.44 ± 0.02
ρ_{CH_2} (e/Å^3)	0.28 ± 0.1		0.30 ± 0.01	0.30 ± 0.01
ρ_{CH_3} (e/Å^3)	0.20 ± 0.1		0.21 ± 0.01	0.21 ± 0.01
Thick	59.6 ± 0.8		47.8 ± 1.0	43.0 ± 0.7
N	3.0 ± 1.0	--	--	--
d (Å)	74.7 ± 0.1	--	--	--
$\eta_{Caillè}$ (x10^{-2})	5.7 ± 0.7	--	--	--

w is the weight of each model, being model 1 the MLV and model 2 the unilamellar one, **R_{pol}** is the polar head thickness; $\boldsymbol{R_{CH_2}}$ is the acyl chain length; $\boldsymbol{R_{CH_3}}$ is the, methyl length; $\boldsymbol{\rho_{pol}}$, $\boldsymbol{\rho_{CH_2}}$ and $\boldsymbol{\rho_{CH_3}}$ are the respective electron densities (being the electron density of the solution equal to $\boldsymbol{\rho_{CH_3}}$ **= 0.333 e/Å^3**); **Thick** is the bilayer thickness; **N** and **d** are the number and average distance among the center-to-center bilayers in one-dimensional lamellar stacking, respectively; $\eta_{Caillé}$ is the Caillé parameter.

The same analysis was performed on nanoL and nanoL-AZ, employing the modified Caillè Theory. Table 3 shows the best fitting parameters related to the solid lines on Figure 2a. SAXS data show curves without statistical differences between nanoL and nanoL -AZ, the fitting parameters thus being also the same. Such finding corroborates with a non (or almost undetectable) interaction of AZ and nanoL bilayer.

3.2 Activity of AZ-nanovesicles against PAO1 and *S. aureus*

Antimicrobial activity of AZ and AZ-nanovesicles on PAO1 and *S. aureus* was measured by determining MIC and MBC on planktonic bacteria and inhibition of biofilm formation. There were also determined their disruptive activity on pre-formed biofilm and the bacterial viability in the biofilm. *S. aureus* was included as an example of Gram-positive species, that together with Gram-negative *P. aeruginosa* and *Burkholderia cenocepacia* are the major opportunistic pathogens implicated in pulmonary infection.[48]

MIC and MBC of AZ and AZ-nanovesicles are shown in Table 4. It was found that, despite of the poor *in vitro* activity reported for AZ against PAO1 the bacteriostatic and bactericidal activities of AZ-nanovesicles on PAO1, were higher than those of AZ.[49] In comparison, an increased bactericidal activity of nanoARC-AZ, higher than those of nanoL-AZ and AZ was found on *S. aureus.* Void nanoL and nanoARC did not show antibacterial activity even up to 2.3 mg TL/mL.

Table 4. MIC and MBC of AZ-nanovesicles on planktonic *S. aureus* and PAO1

	S. aureus		**PAO1**	
Sample	**MIC (µg/mL)**	**MBC (µg/mL)**	**MIC (µg/mL)**	**MBC (µg/mL)**
AZ	4	256	32	64
nanoL-AZ	4	256	16	16
nanoARC-AZ	4	64	8	16

Below the MIC concentration, AZ-nanovesicles partly inhibited PAO1 and *S. aureus* biofilm formation, while AZ had no inhibitory activity (Figure 3a and b).

It was also found that AZ-nanovesicles disrupted the PAO1 biofilm biomass more efficiently than AZ (Figure 4a). Besides, from 32 µg/mL AZ, AZ-nanovesicles displayed higher antibacterial activity in the biofilm than AZ (Figure 4b). No significant differences were found between nanoARC-AZ and

nanoL-AZ. Overall, AZ-nanovesicles had higher antibacterial activity in biofilms and disrupted PAO1 biofilms at lower concentrations than AZ. Neither AZ not AZ-nanovesicles, on the other hand, disrupted the *S. aureus* preformed biofilm (Figure S.2a); this was accompanied by a strong antibacterial activity, that was independent from AZ concentration (Figure S.2b). Since AZ-nanovesicles neither disrupted *S. aureus* biofilm nor displayed higher antibacterial activity than AZ, the following assays were performed only on PAO1.

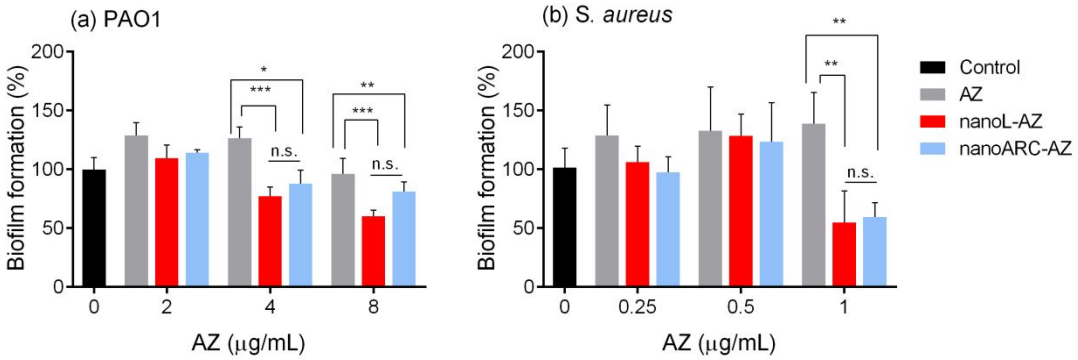

Figure 3. Inhibition of biofilm formation upon 24 h incubation with AZ or AZ-nanovesicles with planktonic PAO1 (a) and *S. aureus* (b).

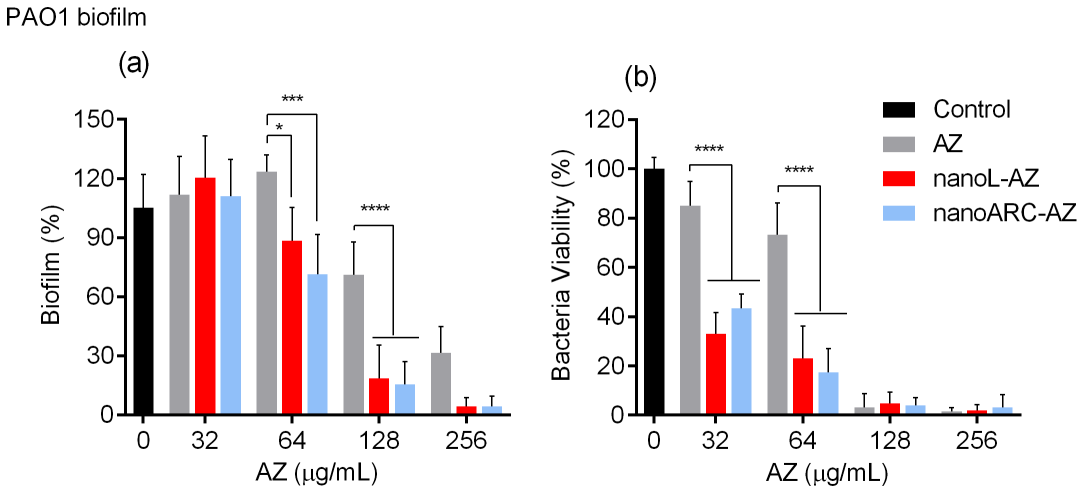

Figure 4. Disruption of preformed biofilm (a) and antibacterial activity (b) of PAO1 upon 24 h incubation with AZ or AZ-nanovesicles.

3.3 Activity of AZ-nanovesicles against PAO1: virulence factors, effect of mucins and biofilm penetration

Different from Solleti et al.,[27] below the MIC concentration (0.5 μg/mL AZ), AZ-nanovesicles did not show higher inhibitory activity of virulence factors (proteases and lipase) than AZ (Figure 5).

The presence of mucins reduced the magnitude of ζ potential of nanoARC-AZ from -35 mV to ~ -9 mV, whereas that of nanoL-AZ remained unaffected (Figure 6c). The mixture of nanoL-AZ and

mucins on the other hand, showed 2 shoulders with maximum in ~75 and ~150 nm, both of size higher than mucins alone and nanoL-AZ alone (Figure 6a). The mixture of nanoARC-AZ and mucins instead, showed two peaks, the one of nanoARC-AZ (~90 nm) and the other corresponding to the medium size of mucins (~30 nm) (Figure 6b). Identical results were observed for mixtures of mucins and void nanovesicles. The reduced ζ potential and size enlargements suggest that upon contact, mucins wrapped nanoARC and nanoL surfaces. Additionally, dropped on the surface of a mucin layer, nanovesicles were observed to penetrate across the media at different speeds; as seen in Figure 6d, nanoL made it faster than nanoARC: 80 % of nanoL crossed the layer in 5 h whereas the same proportion of nanoARC made it in 10 h. In our experimental conditions of ~1x 10^7 bacteria/mL per ~1,88 x 10^8 nanovesicles, roughly estimated assuming 10^3 daltons mean MW of lipids for 150 nm mean sized nanovesicles (S. 3), mucins were observed to increase nanoARC adhesion to PAO1 surface from 10 to 20 %, the same adhesion percentage of nanoL (Figure 7). Mucins finally, slightly decreased the antibacterial activity of AZ-nanovesicles (at 16 μg/mL nanoL-AZ, and at 16 and 32 μg/mL nanoARC-AZ), while that of AZ remained unaffected (Figure 8). Overall, mucins increased the nanoARC-AZ adhesion to PAO1 surface, and slightly reduced their antiPAO1 activity only at low doses of nanoARC-AZ.

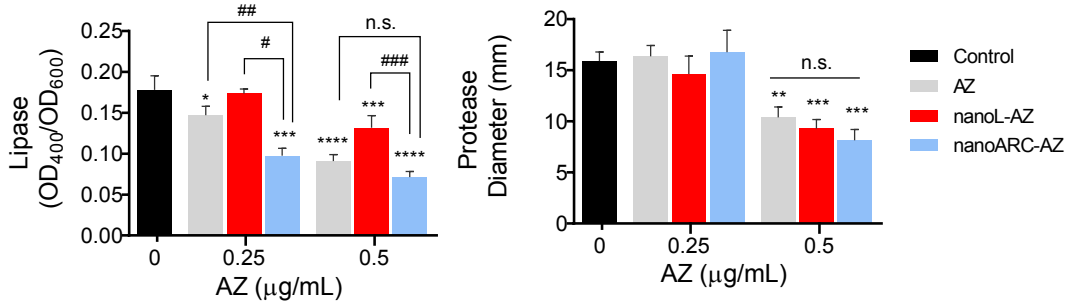

Figure 5. Inhibitory activity of lipase and protease on PAO1 upon incubation with AZ or AZ-nanovesicles. Significant differences with control (*) and between samples (#).

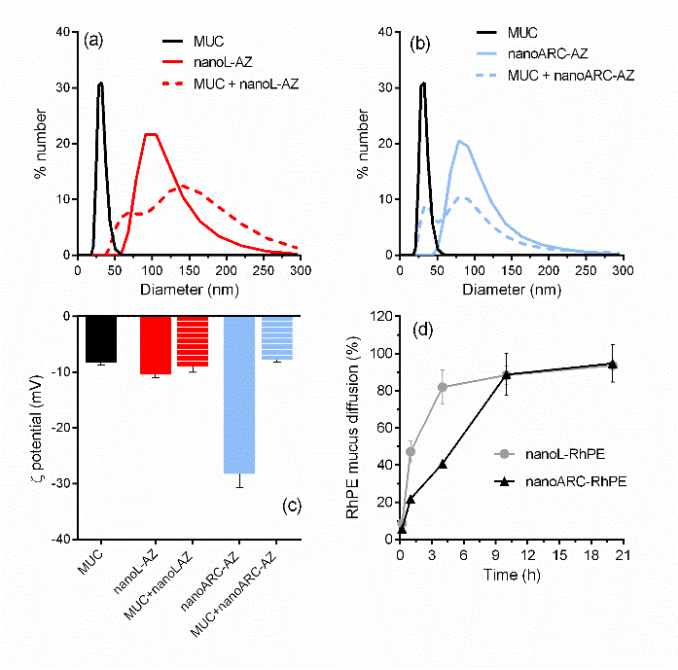

Figure 6. Changes in mean size (a and b) and ζ potential (c) of AZ-nanovesicles upon 60 min contact with mucins (MUC), mucin:nanovesicles 1:1 w:w at 37°C. RhPE-nanovesicles diffusion across a mucin layer within a Transwell system (d).

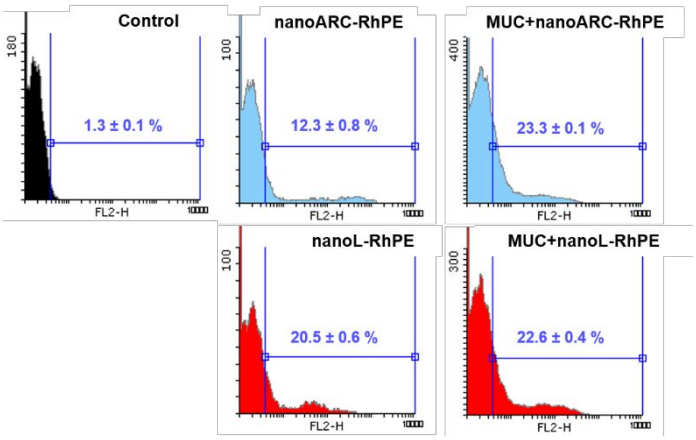

Figure 7. Adhesion of RhPE-nanovesicles on planktonic PAO1 in the presence or absence of mucins (MUC), upon 1 h incubation at 37°C and 250 rpm.

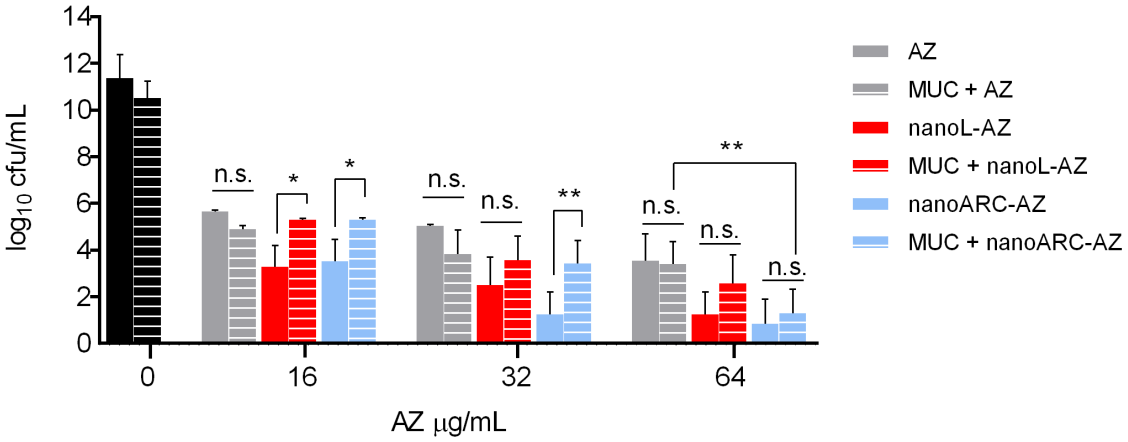

Figure 8. Anti-PAO1 activity of AZ and AZ-nanovesicles in the presence or absence of mucins (MUC) upon 24 h incubation at 37°C.

The confocal fluorescence microscopy images showed that within 1 h the penetration of nanoARC-RhPE in preformed PAO1 biofilms carried ~7 folds more mass [assuming the fluorescent dye was not released, the higher fluorescence intensity across the biofilm depth is indicative of increased mass penetration] than nanoL-RhPE (Figure 9b). In absence of AZ (an antibiotic displaying biofilm disruptive activity), nanoARC-RhPE penetrated the biofilm matrix displaying a homogeneous distribution pattern that co-localized with Hoechst; the lagoons/discontinuities in bacteria organization suggested the occurrence of fast biofilm disruption, exclusively owed to nanoARC bilayers (Figure 9a).[50] The structural disorganization was observed to increase with time, faster and more pronounced by nanoARC-RhPE, less pronounced and slower by nanoL-RhPE upon 24 h (Figure 9c).

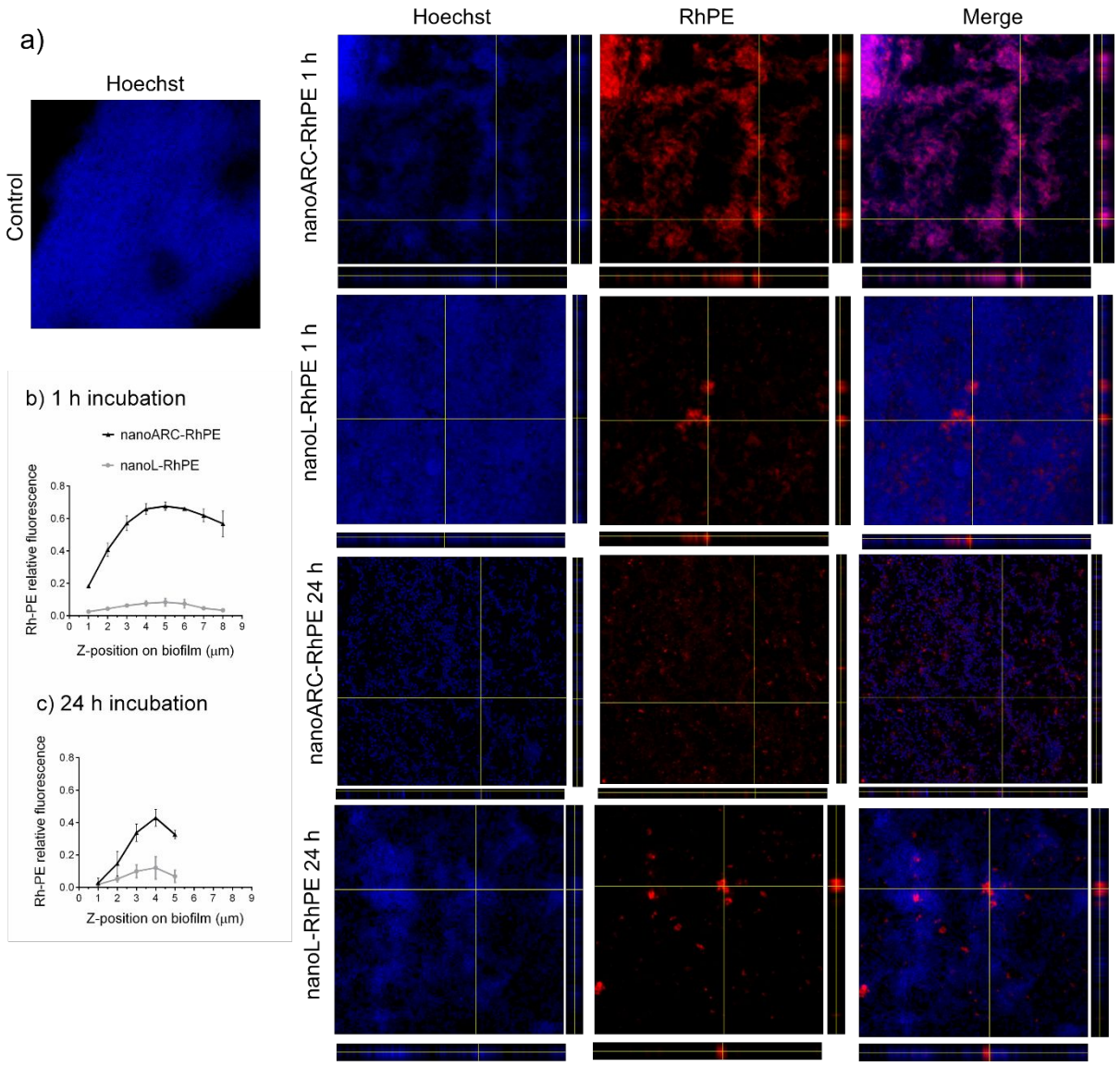

Figure 9. Orthogonal images from confocal microscopy of preformed PAO1 biofilm after 1 and 24 h incubation with nanoARC-RhPE and nanoL-RhPE. Biofilms were stained and visualized using Hoechst. The middle square images are a layer of the biofilm z-stack with the maximum fluorescence intensity of RhPE. The panels on the right and bottom are the y-stack and x-stack respectively (a). Quantification of nanovesicles penetration within PAO1 biofilm after 1 h (b) and 24 h incubation (c), RhPE FI was normalized against Hoechst FI.

3.4 Toxicity of AZ-nanovesicles on human cells

The cytotoxicity of AZ-nanovesicles on A549 and THP-1 cells was determined by the MTT method. Upon 24 h, neither free AZ not AZ-nanovesicles up to 225 μg AZ/mL and 900 μg TL/mL were observed to decrease A549 and THP-1 cells viability (Figure 10 a and b).

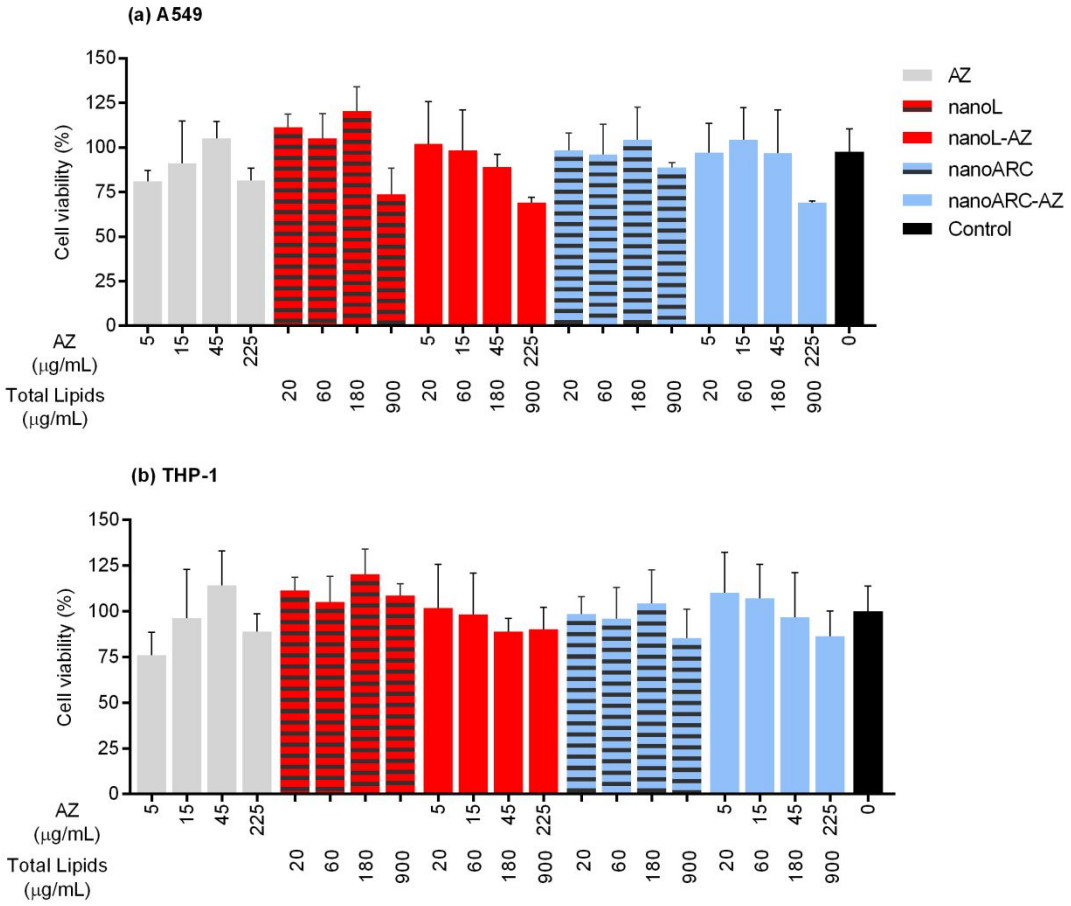

Figure 10. Cell viability measured by MTT upon 24 h incubation with AZ or AZ-nanovesicles on A549 (a) and THP-1 eukaryotic cell lines (b). Samples and control have no significant differences $p > 0.05$.

3.5 Structural stability of AZ-nanovesicles upon nebulization

The ability of nanovesicles to retain colloidal structure against nebulization shear forces, was determined by comparing nanovesicles population size, PDI, AZ and TP content before and after nebulization. It was observed that nebulized nanoL-AZ displayed 6 and 4 folds higher mean size and PDI, respectively, than before nebulization; besides, only 50 % of TL was recovered whereas the total content of AZ was lost (Figure 11). On the other hand, nebulized nanoARC-AZ retained mean size, experiencing a slight increase in PDI, whereas more than 90% of AZ and TL was recovered in the nebulized.

3.6 Structural stability of AZ-nanovesicles upon storage

It was observed that upon 2 months storage at 4°C, the colloidal stability of nanoARC-AZ was higher than that of nanoL-AZ: nanoARC-AZ retained mean population size and PDI, after 6 months these parameters increased in lower extent that for nanoL-AZ (Figure 12).

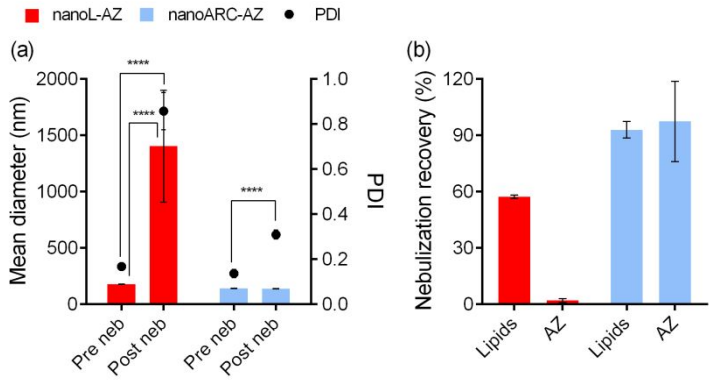

Figure 11. AZ-nanovesicles structural stability upon nebulization (a) and AZ and TL recovery after nebulization (b).

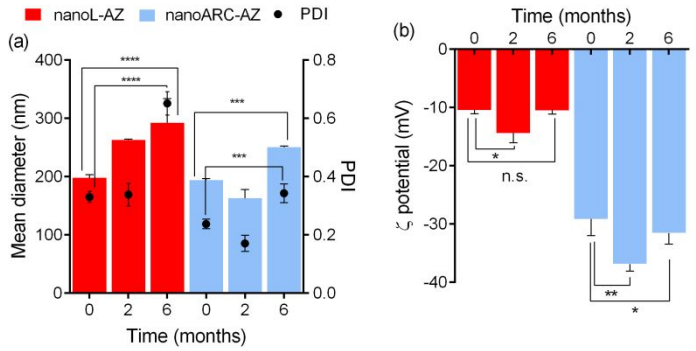

Figure 12. AZ-nanovesicles structural stability upon 2-6 months storage at 4°C.

4. Discussion

This work was aimed to design, characterize the structural features, and screen the antibacterial performance of AZ loaded nanoARC suitable for aerosolization. To the best of our knowledge, it constitutes the first report of an inhalable AZ in lipid nanocarrier.

Here, nanoARC-AZ were prepared employing the simple thin film hydration method; the archaeolipid bilayer trapped AZ, increasing its concentration in aqueous suspension by 760 folds, in a highly stable fashion; nanoL-AZ increased AZ in a comparable extent.

NanoARC-AZ and nanoL-AZ displayed lower MIC and MBC on PAO1, than AZ. The ability of nanovesicles to associate with bacterial surface, as revealed by flow cytometry, would be responsible of the higher biofilm disruptive activity and antibacterial in biofilm activity of AZ-nanovesicles; those were important findings since *P. aeruginosa*, living as a biofilm, was shown to be as much as 1,000 times more resistant to antibiotic treatment than its planktonic counterpart.[51] Previous studies had already showed the fusion/association between liposomes and *Pa* surface.[52] Surface association would reduce the time for released AZ to diffuse from AZ nanovesicles towards the surface of planktonic bacterial bodies. Free AZ instead, bioavailable only at low concentration, would have to diffuse longer distances to get the bacteria surface.

As expected, since planktonic *Pa* in exponential phase are marginally affected by AZ[49], AZ-nanovesicles poorly inhibited the biofilm formation, an assay performed on bacteria growing in exponential phase. In the same trend, below the MIC, neither AZ nor AZ-nanovesicles affected the mobility of planktonic bacteria, whereas nanoARC-AZ barely reduced the production of virulence factor lipases. Instead, opposite to its effect on planktonic bacteria, AZ exerts antibacterial activity against *Pa*

living in stationary phase within biofilms.[49] That explains why AZ nanovesicles more efficiently disrupt the structure of preformed biofilm, and displayed higher antibacterial activity in the biofilm than AZ.

The presence of mucins has been already reported to inhibit the anti-*Pa* activity (32 folds higher MBC) of liposomal aminoglycosides of size comparable to that of AZ-nanovesicles.[53] Opposite to that, we found that mucins would not constitute appreciable barriers neither to the access to bacterial surface not for the antibacterial activity of AZ-nanovesicles. Mucus of the airways may either trap particulate material or the three-dimensional network of mucins polymers may be penetrated by particles.[54] Mucopenetrating nanovesicles access to the deeper mucin layer, being locally retained by longer time than mucoadhesive ones.[55,56] We found here that nanoARC penetrated slower than nanoL across the mucin layer. Because of their comparable size (~ 150 nm), the slowness of nanoARC could be ascribed to a higher interaction by hydrogen bonding between surface sugars headgroups from TPA in nanoARC and mucins.[54] Additionally, mucins neither decreased the association between AZ nanovesicles and PAO1 surface, nor their antimicrobial activities. The exception occurred with low AZ nanovesicles concentration, where their antibacterial activity decreased toward that of AZ. This fact suggests that below a threshold of AZ-nanovesicles/bacteria ratio (at 64 μg/mL for nanoARC-AZ), mucins hampered the association of AZ-nanovesicles to bacterial surface. Hence, AZ released from distant non-associated AZ nanovesicles, had to diffuse longer distance across the media, to get bacterial surface. Even so, the CFU/mL resultant from 64 μg/mL nanoARC-AZ was inferior to that of AZ. This could be owed to the highly concentrated AZ depot character of nanoARC-AZ, whose AZ release profile into the bacterial microenvironment, would kill it more efficiently than AZ or nanoL-AZ.

We observed overall, that despite of improving the effect of AZ, no significant differences were found between nanoARC-AZ and nanoL-AZ in terms of AZ/lipids ratio, MIC, MBC, PA surface association mucopenetration, biofilm disruption and bactericidal activity within the biofilms. Despite of that, in this work 3 competitive advantages of nanoARC matrix compared to nanoL, were revealed. The first was the ability of nanoARC to quickly penetrate a preformed biofilm of PAO1. Within 1-hour nanoARC penetrated deeper and in higher extent than nanoL. NanoL on the other hand, was observed to be aggregated along penetration. It took 24 h the biofilm disruptive activity of nanoL to became comparable to that of nanoARC, though repeating the less penetrating pattern. The two reminder advantages resulted from the interaction between nanoARC bilayer and AZ. Archaeolipids composing nanoARC bilayers, are amphipathic cylindrical molecules having *sn*2,3 polyisoprenoid chains bonded by ether linkages to the glycerol backbone. Methyl groups perpendicular to the longitudinal molecule axis, are responsible for the high transverse area of archaeolipids and features such as high disorder of the low lateral mobility bilayers.[57] The archaeolipids architecture mimics that of isostearic acid, a fatty esters mixture consisting mainly of methyl branched isomers of octadecanoic acid used as surfactant, cleanser and binder in pharmaceutics and cosmetics.[58] Importantly, the main component of *H. tebenquichense* polar lipids, is the 2,3-di-O-phytanyl-snglycero-1-phospho-(3'-sn-glycerol-1'-methylphosphate) (PGP-Me), an archaeolipid displaying a double negative charge at physiological pH, that is also a ligand for SRA1. PGP-Me containing nanoARC therefore, are naturally targeted to cells expressing SRA1. The combination of such unique biophysical and pharmacodynamics features of nanoARC bilayers, was recently exploited to trap difficult to dissolve in water drugs, such as the immunomodulator imiquimod.[59]

Despite of the AZ: lipid w:w ratios of nanoARC-AZ (0.28) (vs (0.20) from nanoL-AZ nanoliposomes made of ordinary phospholipids used as a control) were comparable and in the order of those previously reported for other AZ vesicular formulations (~0.24[27] and ~0.23[60]), the interaction between AZ and nanoARC bilayers was unique, and different from that occurring within nanoliposomes, where AZ remained dissolved/precipitated within the aqueous space. The ζ potential values, together with the structural data provided by GP, FA and SAXS, showed that AZ associated to nanoARC bilayers consisted of a combination of electrostatic interaction between negatively charged nanoARC surface and the two tertiary amines of ~ 8.7 and ~ 9.3 pKa from dicationic AZ[61] with trapping within the interface and the inner most methyl groups. The nature of AZ association was key to define the structural stability of nanoARC-AZ upon storage and nebulization stress.

Opposite to nanoL-AZ, nanoARC-AZ experienced minimal increased size and PDI after 6 months at 4°C. This is important because enlarged nanovesicles, besides of losing inner content, may experience hampered mucopenetration[56] and biofilm penetration[45]. The second advantage was thus the higher stability of nanoARC-AZ during storage. But the last and most important one, was that only nanoARC-AZ were structurally stable to nebulization stress**.** The aqueous suspensions of AZ

nanovesicles exhibited comparable anti-PAO1 activity. Upon nebulization however, the structural lability of nanoL-AZ made them polydisperse, enlarged and depleted from AZ, presumably, upon the action of shear forces needed to produce nebulized water microdroplets.[62,63] Instead, negatively charged PGP-Me in nanoARC-AZ bilayer, attracted positively charged AZ; that interaction, combined with physical trapping within archaeolipid bilayer, maintained the association between AZ and archaeolipid matrix during bilayer disruption along nebulization. Liposomal antibiotics are known to display higher antibacterial activity on biofilms than free antibiotic, because of their ability to penetrate the biofilm structure. The prolonged contact with liposomal depots from where antibiotic is released, results in an improved activity against bacteria in biofilm.[64,65]

A study published 2006 showed that Zithromax, an injectable highly concentrated AZ aqueous solution, could be aerosolized employing jet nebulizers.[17] Because of the low water solubility of AZ base (0.0025 mg/mL at 25° C)[66], the AZ dihydrate used in such injectable solution requires of massive amounts of citric acid and sodium hydroxide as inactive ingredients.[67] Theoretically, injectable formulations of AZ can be nebulized.[68] In practice however, preservatives and admixtures comprised in injectable formulations may cause bronchospasm, cough, or occlusion of the expiratory filter and contribute to suboptimal drug deposition.[69] Upon nebulizing a 100 mg AZ/mL dilution of Zithromax, the emitted AZ concentration was reduced to nearly the half, 55 mg AZ/mL. The poor stability of highly concentrated AZ solutions (only 24 h at T < 30°C), together with high salt concentrations led to AZ precipitation and clogging (as suggested by the reduced AZ emitted dose), probably hampering a succeeding nebulization. No further reports on nebulized AZ were published in the last twelve years, probably because of these drawbacks.

In this work, 2 mL of 15 µg/mL nanoARC-AZ were nebulized along 5 min at 0.25 mL/min, resulting a dose of nearly 30 µg AZ per 110 µg lipids. This is a relatively diluted suspension of AZ compared to the used by Hickey et al., 2006[17], nearly 6,600 folds higher. However, different to AZ or nanoL-AZ, nanoARC-AZ could be conserved as a stable suspension to be nebulized without visible clogging of the vibrating mesh, retaining the association between AZ and nanoARC. The nanoARC matrix deeply and homogeneously penetrated the PAO1 biofilms, nanoARC-AZ being efficient antibacterial agent at doses compatible with 5 minutes nebulization.

5. Conclusions

Ordinary lipid bilayers such as that made of 3:1 w: w HSPC:Chol used in this work, are unsuitable as nebulized AZ nanocarriers. The novelty presented here is that nanoARC bilayers, lacking Chol cholesterol and artificially hydrogenated lipids, may be successfully used as nebulized AZ nanocarriers. NanoARC thus, may result as suitable alternative to the nebulized hard liposomes in advanced clinical trials and recently approved by the FDA.[19-22] The efficient association between AZ and nanoARC bilayer, was maintained against shear forces of nebulization: nanoARC-AZ remained structurally stable in suspension along storage, and AZ remained trapped into nanoARC bilayer with no need of highly concentrated acids and bases. *In vivo*, because of being SRA1 targeted formulations, nanoARC-AZ may have synergic immunomodulatory effects, aiding to reduce the inflammation associated to chronic inflammation. NanoARC-AZ, the first nebulized AZ-nanovesicle formulation, enhanced the anti-PAO1 activity of AZ at doses below the cytotoxicity on A549 cells and human THP-1 derived macrophages. Deeper insights on the effect of nebulized nanoARC-AZ, a formulation that combines bacteriostatic/bactericidal activity with SRA1 targeting, deserve to be explored on a suitable disease model.

Acknowledgements

This work was supported by Secretaria de Investigaciones, Universidad Nacional de Quilmes under Grant Nanomedicinas-2. MJA and MMBM has fellowships from National Council for Scientific and Technological Research (CONICET). ELR, MJM and PCM are members of the Research Career Program from CONICET.

Supporting Information

Mathematical aspects of SAXS, activity of AZ-nanovesicles against *S. aureus* and estimation of the number of vesicles.

References

1. Dunn, C. J.; Barradell, L. B., Azithromycin. *Drugs* **1996,** *51* (3), 483-505.
2. Prescott Jr, W. A.; Johnson, C. E., Antiinflammatory therapies for cystic fibrosis: past, present, and future. *Pharmacotherapy: The Journal of Human Pharmacology and Drug Therapy* **2005,** *25* (4), 555-573.
3. Zimmermann, P.; Ziesenitz, V. C.; Curtis, N.; Ritz, N., The immunomodulatory effects of macrolides—A systematic review of the underlying mechanisms. *Frontiers in immunology* **2018,** *9*, 302.
4. Döring, G.; Flume, P.; Heijerman, H.; Elborn, J. S.; Group, C. S., Treatment of lung infection in patients with cystic fibrosis: current and future strategies. *Journal of Cystic Fibrosis* **2012,** *11* (6), 461-479.
5. Southern, K. W.; Barker, P. M.; Solis-Moya, A.; Patel, L., Macrolide antibiotics for cystic fibrosis. *Cochrane Database of Systematic Reviews* **2004,** (2).
6. Aminov, R. I., Biotic acts of antibiotics. *Frontiers in microbiology* **2013,** *4*, 241.
7. Neu, H. C., The role of Pseudomonas aeruginosa in infections. *Journal of Antimicrobial Chemotherapy* **1983,** *11* (suppl_B), 1-13.
8. Wood, R., t TF, Doerohak CF. *Cysttc flbrosls. Am Rev Resplr Dis* **1976,** *113*, 833-78.
9. Homma, H.; Yamanaka, A.; Tanimoto, S.; Tamura, M.; Chijimatsu, Y.; Kira, S.; Izumi, T., Diffuse panbronchiolitis: a disease of the transitional zone of the lung. *Chest* **1983,** *83* (1), 63-69.
10. Finch, S.; McDonnell, M. J.; Abo-Leyah, H.; Aliberti, S.; Chalmers, J. D., A comprehensive analysis of the impact of Pseudomonas aeruginosa colonization on prognosis in adult bronchiectasis. *Annals of the American Thoracic Society* **2015,** *12* (11), 1602-1611.
11. Mogayzel Jr, P. J.; Naureckas, E. T.; Robinson, K. A.; Mueller, G.; Hadjiliadis, D.; Hoag, J. B.; Lubsch, L.; Hazle, L.; Sabadosa, K.; Marshall, B., Cystic fibrosis pulmonary guidelines: chronic medications for maintenance of lung health. *American journal of respiratory and critical care medicine* **2013,** *187* (7), 680-689.
12. Kasahara, K.; Maeda, K.; Mikasa, K.; Uno, K.; Takahashi, K.; Konishi, M.; Yoshimoto, E.; Murakawa, K.; Kimura, H.; Kita, E., Longterm azithromycin therapy for three patients with chronic lower respiratory tract infections. *Journal of infection and chemotherapy* **2004,** *10* (1), 42-45.
13. Wang, Q.; Mi, G.; Hickey, D.; Li, Y.; Tu, J.; Webster, T. J.; Shen, Y., Azithromycin-loaded respirable microparticles for targeted pulmonary delivery for the treatment of pneumonia. *Biomaterials* **2018,** *160*, 107-123.
14. Heijerman, H.; Westerman, E.; Conway, S.; Touw, D.; group, G. D. f. t. c. w., Inhaled medication and inhalation devices for lung disease in patients with cystic fibrosis: a European consensus. *Journal of Cystic Fibrosis* **2009,** *8* (5), 295-315.
15. Cantin, A. M.; Hartl, D.; Konstan, M. W.; Chmiel, J. F., Inflammation in cystic fibrosis lung disease: pathogenesis and therapy. *Journal of Cystic Fibrosis* **2015,** *14* (4), 419-430.
16. Liu, P.; Allaudeen, H.; Chandra, R.; Phillips, K.; Jungnik, A.; Breen, J. D.; Sharma, A., Comparative pharmacokinetics of azithromycin in serum and white blood cells of healthy subjects receiving a single-dose extended-release regimen versus a 3-day immediate-release regimen. *Antimicrobial agents and chemotherapy* **2007,** *51* (1), 103-109.
17. Hickey, A. J.; Lu, D.; Ashley, E. D.; Stout, J., Inhaled azithromycin therapy. *Journal of aerosol medicine* **2006,** *19* (1), 54-60.
18. Choi, Y. H.; Han, H.-K., Nanomedicines: current status and future perspectives in aspect of drug delivery and pharmacokinetics. *Journal of pharmaceutical investigation* **2018,** *48* (1), 43-60.
19. Cipolla, D.; Blanchard, J.; Gonda, I., Development of liposomal ciprofloxacin to treat lung infections. *Pharmaceutics* **2016,** *8* (1), 6.
20. Corporation, A. http://www.aradigm.com/products_pipeline.html (accessed April 2019).

21. Bilton, D.; Pressler, T.; Fajac, I.; Clancy, J. P.; Sands, D.; Minic, P.; Cipolli, M.; LaRosa, M.; Galeva, I.; Sole, A. A., Phase 3 efficacy and safety data from randomized, multicenter study of liposomal amikacin for inhalation (ARIKACE) Compared with TOBI in cystic fibrosis patients with chronic infection due to Pseudomonas Aeruginosa. *Pediatr Pulmonol* **2013,** *48* (S36), 207-453.
22. O'Donnell, A.; Swarnakar, R.; Yahina, L., A placebo-controlled study of liposomal amikacin for inhalation nebulized once daily in the treatment of bronchiectasis patients with chronic Pseudomonas aeruginosa lung infection. *Eur Respir J* **2009,** *34* (Suppl 53), 1361.
23. Insimed, I. https://www.insmed.com/arikayce/ (accessed April 2019).
24. Hadinoto, K.; Cheow, W. S., Nano-antibiotics in chronic lung infection therapy against Pseudomonas aeruginosa. *Colloids and Surfaces B: Biointerfaces* **2014,** *116*, 772-785.
25. Cassidy, J. P.; Amin, N.; Marino, M.; Gotfried, M.; Meyer, T.; Sommerer, K.; Baughman, R. A., Insulin lung deposition and clearance following Technosphere® insulin inhalation powder administration. *Pharmaceutical research* **2011,** *28* (9), 2157-2164.
26. Kaur, N.; Zhou, B.; Breitbeil, F.; Hardy, K.; Kraft, K. S.; Trantcheva, I.; Phanstiel Iv, O., A Delineation of Diketopiperazine Self-Assembly Processes: Understanding the Molecular Events Involved in N ϵ-(Fumaroyl) diketopiperazine of l-Lys (FDKP) Interactions. *Molecular pharmaceutics* **2008,** *5* (2), 294-315.
27. Solleti, V. S.; Alhariri, M.; Halwani, M.; Omri, A., Antimicrobial properties of liposomal azithromycin for Pseudomonas infections in cystic fibrosis patients. *Journal of Antimicrobial Chemotherapy* **2014,** *70* (3), 784-796.
28. Clancy, J.; Dupont, L.; Konstan, M.; Billings, J.; Fustik, S.; Goss, C.; Lymp, J.; Minic, P.; Quittner, A.; Rubenstein, R., Phase II studies of nebulised Arikace in CF patients with Pseudomonas aeruginosa infection. *Thorax* **2013,** *68* (9), 818-825.
29. List, G. R.; King, J. W., *Hydrogenation of fats and oils: Theory and practice*. Elsevier: 2016.
30. Corcelli, A.; Lobasso, S., 25 characterization of lipids of halophilic archaea. In *Methods in microbiology*, Elsevier: 2006; Vol. 35, pp 585-613.
31. Schilrreff, P.; Simioni, Y. R.; Jerez, H. E.; Caimi, A. T.; de Farias, M. A.; Portugal, R. V.; Romero, E. L.; Morilla, M. J., Superoxide dismutase in nanoarchaeosomes for targeted delivery to inflammatory macrophages. *Colloids and Surfaces B: Biointerfaces* **2019**.
32. Altube, M. J.; Selzer, S. M.; de Farias, M. A.; Portugal, R. V.; Morilla, M. J.; Romero, E. L., Surviving nebulization-induced stress: dexamethasone in pH-sensitive archaeosomes. *Nanomedicine* **2016,** *11* (16), 2103-2117.
33. Gonzalez, R. O.; Higa, L. H.; Cutrullis, R. A.; Bilen, M.; Morelli, I.; Roncaglia, D. I.; Corral, R. S.; Morilla, M. J.; Petray, P. B.; Romero, E. L., Archaeosomes made of Halorubrum tebenquichense total polar lipids: a new source of adjuvancy. *BMC biotechnology* **2009,** *9* (1), 71.
34. Kates, M.; Kushwaha, S., Isoprenoids and polar lipids of extreme halophiles. *Archaea, a laboratory manual. Halophiles. Cold Spring Harbor Laboratory Press, Cold Spring Harbor* **1995**, 35-54.
35. Biittcher, C.; Van Gent, C.; Pries, C., A rapid and sensitive sub-micro-phosphorus determination. *Anal Chim Acta* **1961,** *24*, 203-204.
36. Higa, L. H.; Schilrreff, P.; Perez, A. P.; Iriarte, M. A.; Roncaglia, D. I.; Morilla, M. J.; Romero, E. L., Ultradeformable archaeosomes as new topical adjuvants. *Nanomedicine: Nanotechnology, Biology and Medicine* **2012,** *8* (8), 1319-1328.
37. Haleem, D.; Shireen, E.; Haleem, M.; Kaye, W.; Bailer, U.; Frank, G.; Wagner, A.; Henry, S., Degradation studies of azithromycin and its spectrophotometric determination in pharmaceutical dosage forms. *Pak. J. Pharm. Sci* **2006,** *19* (2), 98-103.
38. Domingues, M. M.; Bianconi, M. L.; Barbosa, L. R.; Santiago, P. S.; Tabak, M.; Castanho, M. A.; Itri, R.; Santos, N. C., rBPI21 interacts with negative membranes endothermically promoting the

formation of rigid multilamellar structures. *Biochimica et Biophysica Acta (BBA)-Biomembranes* **2013,** *1828* (11), 2419-2427.

39. Rozenfeld, J. H.; Duarte, E. L.; Barbosa, L. R.; Lamy, M. T., The effect of an oligonucleotide on the structure of cationic DODAB vesicles. *Physical Chemistry Chemical Physics* **2015,** *17* (11), 7498-7506.

40. Institute, C. a. L. S., Methods for antimicrobial susceptibility testing of anaerobic bacteria. 2012; Vol. M11-A8.

41. Jin, F.; Welch, R.; Glahn, R., Moving toward a more physiological model: application of mucin to refine the in vitro digestion/Caco-2 cell culture system. *Journal of agricultural and food chemistry* **2006,** *54* (23), 8962-8967.

42. Nafee, N.; Husari, A.; Maurer, C. K.; Lu, C.; de Rossi, C.; Steinbach, A.; Hartmann, R. W.; Lehr, C.-M.; Schneider, M., Antibiotic-free nanotherapeutics: ultra-small, mucus-penetrating solid lipid nanoparticles enhance the pulmonary delivery and anti-virulence efficacy of novel quorum sensing inhibitors. *Journal of controlled release* **2014,** *192*, 131-140.

43. Friedl, H.; Dünnhaupt, S.; Hintzen, F.; Waldner, C.; Parikh, S.; Pearson, J. P.; Wilcox, M. D.; Bernkop-Schnürch, A., Development and evaluation of a novel mucus diffusion test system approved by self-nanoemulsifying drug delivery systems. *Journal of pharmaceutical sciences* **2013,** *102* (12), 4406-4413.

44. Higa, L. H.; Jerez, H. E.; de Farias, M. A.; Portugal, R. V.; Romero, E. L.; Morilla, M. J., Ultra-small solid archaeolipid nanoparticles for active targeting to macrophages of the inflamed mucosa. *Nanomedicine* **2017,** *12* (10), 1165-1175.

45. Dong, D.; Thomas, N.; Thierry, B.; Vreugde, S.; Prestidge, C. A.; Wormald, P.-J., Distribution and Inhibition of Liposomes on Staphylococcus aureus and Pseudomonas aeruginosa Biofilm. *PLoS One* **2015,** *10* (6), e0131806.

46. Schindelin, J.; Arganda-Carreras, I.; Frise, E.; Kaynig, V.; Longair, M.; Pietzsch, T.; Preibisch, S.; Rueden, C.; Saalfeld, S.; Schmid, B., Fiji: an open-source platform for biological-image analysis. *Nature methods* **2012,** *9* (7), 676.

47. da Costa-Silva, T. A.; Galisteo, A. J.; Lindoso, J. A. L.; Barbosa, L. R.; Tempone, A. G., Nanoliposomal buparvaquone immunomodulates Leishmania infantum-infected macrophages and is highly effective in a murine model. *Antimicrobial agents and chemotherapy* **2017,** *61* (4), e02297-16.

48. Bosch, A. A.; Biesbroek, G.; Trzcinski, K.; Sanders, E. A.; Bogaert, D., Viral and bacterial interactions in the upper respiratory tract. *PLoS pathogens* **2013,** *9* (1), e1003057.

49. Imamura, Y.; Higashiyama, Y.; Tomono, K.; Izumikawa, K.; Yanagihara, K.; Ohno, H.; Miyazaki, Y.; Hirakata, Y.; Mizuta, Y.; Kadota, J.-i., Azithromycin exhibits bactericidal effects on Pseudomonas aeruginosa through interaction with the outer membrane. *Antimicrobial agents and chemotherapy* **2005,** *49* (4), 1377-1380.

50. Co, J. Y.; Cárcamo-Oyarce, G.; Billings, N.; Wheeler, K. M.; Grindy, S. C.; Holten-Andersen, N.; Ribbeck, K., Mucins trigger dispersal of Pseudomonas aeruginosa biofilms. *NPJ biofilms and microbiomes* **2018,** *4* (1), 23.

51. Nickel, J.; Ruseska, I.; Wright, J.; Costerton, J., Tobramycin resistance of Pseudomonas aeruginosa cells growing as a biofilm on urinary catheter material. *Antimicrobial agents and chemotherapy* **1985,** *27* (4), 619-624.

52. Mugabe, C.; Halwani, M.; Azghani, A. O.; Lafrenie, R. M.; Omri, A., Mechanism of enhanced activity of liposome-entrapped aminoglycosides against resistant strains of Pseudomonas aeruginosa. *Antimicrobial agents and chemotherapy* **2006,** *50* (6), 2016-2022.

53. Alipour, M.; Suntres, Z. E.; Omri, A., Importance of DNase and alginate lyase for enhancing free and liposome encapsulated aminoglycoside activity against Pseudomonas aeruginosa. *Journal of Antimicrobial Chemotherapy* **2009,** *64* (2), 317-325.

54. Netsomboon, K.; Bernkop-Schnürch, A., Mucoadhesive vs. mucopenetrating particulate drug delivery. *European Journal of Pharmaceutics and Biopharmaceutics* **2016,** *98*, 76-89.
55. Savla, R.; Minko, T., Nanotechnology approaches for inhalation treatment of fibrosis. *Journal of drug targeting* **2013,** *21* (10), 914-925.
56. Schneider, C. S.; Xu, Q.; Boylan, N. J.; Chisholm, J.; Tang, B. C.; Schuster, B. S.; Henning, A.; Ensign, L. M.; Lee, E.; Adstamongkonkul, P., Nanoparticles that do not adhere to mucus provide uniform and long-lasting drug delivery to airways following inhalation. *Science advances* **2017,** *3* (4), e1601556.
57. Kitano, T.; Onoue, T.; Yamauchi, K., Archaeal lipids forming a low energy-surface on air-water interface. *Chemistry and physics of lipids* **2003,** *126* (2), 225-232.
58. Cosmeticsinfo.org https://cosmeticsinfo.org/ingredient/isostearic-acid-0 (accessed April 2019).
59. Parra, F. L.; Caimi, A. T.; Altube, M. J.; Cargnelutti, D. E.; Vermeulen, M. E.; de Farias, M. A.; Portugal, R. V.; Morilla, M. J.; Romero, E. L., Make it simple:(SR-A1+ TLR7) macrophage targeted NANOarchaeosomes. *Frontiers in Bioengineering and Biotechnology* **2018,** *6*.
60. Oh, Y.-K.; Nix, D. E.; Straubinger, R. M., Formulation and efficacy of liposome-encapsulated antibiotics for therapy of intracellular Mycobacterium avium infection. *Antimicrobial agents and chemotherapy* **1995,** *39* (9), 2104-2111.
61. Mandić, Z., Voltammetric study of the partitioning of macrolide antibiotics at the water/nitrobenzene interface. Relationship to the pharmacokinetic profiling of macrolides. *ADMET and DMPK* **2014,** *2* (3), 168-178.
62. Cipolla, D.; Gonda, I.; Chan, H.-K., Liposomal formulations for inhalation. *Therapeutic delivery* **2013,** *4* (8), 1047-1072.
63. Lehofer, B.; Bloder, F.; Jain, P. P.; Marsh, L. M.; Leitinger, G.; Olschewski, H.; Leber, R.; Olschewski, A.; Prassl, R., Impact of atomization technique on the stability and transport efficiency of nebulized liposomes harboring different surface characteristics. *European Journal of Pharmaceutics and Biopharmaceutics* **2014,** *88* (3), 1076-1085.
64. Halwani, M.; Yebio, B.; Suntres, Z.; Alipour, M.; Azghani, A.; Omri, A., Co-encapsulation of gallium with gentamicin in liposomes enhances antimicrobial activity of gentamicin against Pseudomonas aeruginosa. *Journal of Antimicrobial Chemotherapy* **2008,** *62* (6), 1291-1297.
65. Meers, P.; Neville, M.; Malinin, V.; Scotto, A.; Sardaryan, G.; Kurumunda, R.; Mackinson, C.; James, G.; Fisher, S.; Perkins, W., Biofilm penetration, triggered release and in vivo activity of inhaled liposomal amikacin in chronic Pseudomonas aeruginosa lung infections. *Journal of Antimicrobial Chemotherapy* **2008,** *61* (4), 859-868.
66. Aucamp, M.; Odendaal, R.; Liebenberg, W.; Hamman, J., Amorphous azithromycin with improved aqueous solubility and intestinal membrane permeability. *Drug development and industrial pharmacy* **2015,** *41* (7), 1100-1108.
67. FDA https://www.accessdata.fda.gov/drugsatfda_docs/label/2007/050733s018lbl.pdf (accessed April 2018).
68. Poulakou, G.; Siakallis, G.; Tsiodras, S.; Arfaras-Melainis, A.; Dimopoulos, G., Nebulized antibiotics in mechanically ventilated patients: roadmap and challenges. *Expert review of anti-infective therapy* **2017,** *15* (3), 211-229.
69. Mojoli, F.; Iotti, G. A.; Imberti, R.; Braschi, A., The importance of protecting the mechanical ventilator during colistin methanesulfonate nebulization. *Intensive care medicine* **2013,** *39* (3), 535-536.